We are IntechOpen, the world's leading publisher of Open Access books Built by scientists, for scientists

6,900
Open access books available

185,000
International authors and editors

200M
Downloads

Our authors are among the

154
Countries delivered to

TOP 1%
most cited scientists

12.2%
Contributors from top 500 universities



WEB OF SCIENCE™

Selection of our books indexed in the Book Citation Index in Web of Science™ Core Collection (BKCI)

Interested in publishing with us?
Contact book.department@intechopen.com

Numbers displayed above are based on latest data collected.
For more information visit www.intechopen.com



20

Inter-cell Interference Mitigation for Mobile Communication System

Xiaodong Xu[1], Hui Zhang[2] and Qiang Wang[1]
[1]*Wireless Technology Innovation Institute; Key Laboratory of Universal Wireless Comm., Ministry of Education; Beijing University of Posts and Telecommunications,*
[2]*Nankai University*
China

1. Introduction

With the commercialization of 3G mobile communication systems, the ability to provide diversiform data services, high mobility vehicle communication experiences and asymmetrical services are enhanced further than 2G systems. But at the same time, users still have higher requirement for high-rate and high-QoS mobile services. Many international standardization organizations have launched the research and standardization of 3G evolution system, such as 3GPP Long Term Evolution (LTE) and LTE Advanced project. The primary three standards of 3G are all based on Code Division Multiple Access (CDMA), but with the in-depth research of Orthogonal Frequency Division Multiplexing (OFDM) techniques, OFDM has been emphasized by the mobile communication industry and used as the basic multiple access technique in the Enhanced 3G (E3G) systems for its merit of high spectrum efficiency.

OFDM becomes a key technology in the next cellular mobile communication system. As the sub-carriers in the intra-cell are orthogonal with each other, the intra-cell interference can be avoided efficiently. However, the inter-cell interference problems may become serious since many co-frequency sub-carriers are reused among different cells. Under this background, how to mitigate inter-cell interference and improve the performance for cellular users for vehicular environments become more urgent.

In this chapter, the research outcomes about Intel-cell Interference Mitigation technologies and corresponding performance evaluation results will be provided. The Intel-cell Interference Mitigation strategies introduced here will include three categories, which are interference coordination, interference prediction and interference cancellation respectively.

2. Inter-cell interference coordination

Frequency coordination plays important roles in the Inter-cell Interference Coordination scheme. For frequency coordination, one frequency reuse based Interference Coordination scheme will be introduced, called as Soft Fractional Frequency Reuse (SFFR). Its frequency reuse factor will be derived. Simulation results will be provided to show the throughputs in cell-edge are efficiently improved compared with soft frequency reuse (SFR) scheme.

Especially, for Coordinated Multi-point (CoMP) transmission technology, which is the promising technique in LTE-Advanced, a novel frequency reuse scheme – Coordinated Frequency Reuse (CFR) will be introduced, which can support coordination transmission in CoMP system. Simulation results are also provided to show that this scheme enables to improve the throughputs in cell-edge.

2.1 Soft fractional frequency reuse

In order to improve the performance in cell-edge, the SFFR scheme is introduced, which is based on soft frequency reuse. As shown in Fig.1, the characteristics of such reuse schemes are given as follows: the whole cell is divided into two parts, cell-centre and cell-edge. In cell-centre, the frequency reuse factor (FRF) is set as 1, while in cell-edge, FRF is dynamic and the frequency allocation is orthogonal with the edge of other cells, which can avoid partial inter-cell interference in cell-edge.

Specially, users in each cell are divided into two major groups according to their geometry factors. In cell-edge group, users are interference-limited due to the neighbouring cells, whereas in cell-centre group users are mainly noise-limited. The available frequency resources in cell-edge are divided into non-crossing subsets in SFFR.

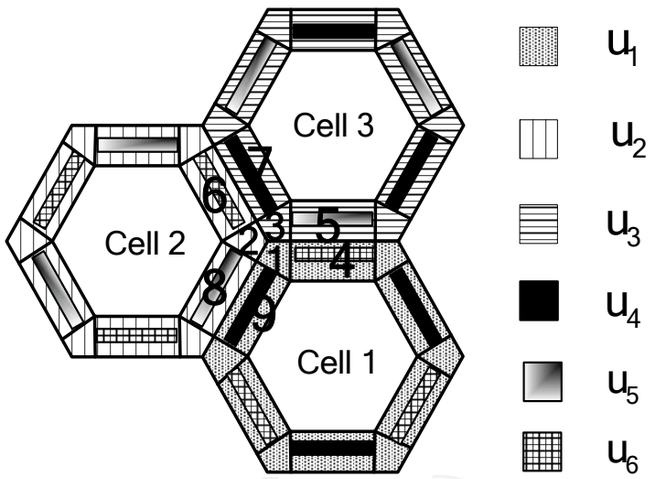


Fig. 1. Concept of Soft Fractional Frequency Reuse

The set of available frequency resources in the cell is allocated as follows: the whole frequency band is divided into two disjoint sub-bands, G and F, where G is allocated to the cell-centre users and F to the cell-edge users. Considering a cluster of 3 cells, as the one shown in Fig. 1, let $F = F_1 \bigcup F_2 \bigcup F_3$, where F_i denotes the subset of frequencies allocated to cell i, $(i = 1,2,3)$, and the subsets F_i may be overlapped with each other.

Since the cell-edge users are easily subject to co-frequency interference, the frequency assignments to the cell-edge users greatly rely on radio link performance and system throughput. Generally, the cell-edge can be divided into 12 regions, as the ones marked by 1, 4, and 9 in Cell 1 (see Fig. 1). Therefore, in a cluster of 3 adjacent cells, there are 9 parts in the cell-edge corner, which are in the shaded area. Moreover, we take this SFFR model as an example to deduce the design of the available frequency band assignment for the fields marked by 1, 2, .., 9.

In SFFR, all the available frequencies in cell-edge are divided into 6 non-overlapping subsets. Such subsets are respectively u_1, u_2, u_3, u_4, u_5 and u_6, while the subset in cell-centre is u_0. Firstly, we select frequency from the subsets u_1, u_2, u_3. If it's not enough, choose frequency from u_4, u_5, u_6. If the inter-cell interference increases, we need to add frequency into u_4, u_5, u_6, and decrease the cover area in cell-edge. If such interference is controlled in a low extension, we can decrease the frequency in subsets of u_4, u_5, u_6, and increase the cover area in cell-edge, which enables to improve the frequency utilization. Moreover, we assume $A_{1/3}=\{u_1,u_2,u_3\}$, $A_{2/3}=\{u_4,u_5,u_6\}$ and $A_{3/3}=\{u_0\}$, where $A_{1/3}$ denotes the frequency set with 1/3 reuse, $A_{2/3}$ denotes the frequency set with 2/3 reuse and $A_{3/3}$ denotes the frequency set with FRF equals to 1.

According to the definition of FRF in references, the FRF of SFFR scheme can be obtained as follows:

$$\eta=\frac{\frac{1}{3}\left|A_{1/3}\right|+\frac{2}{3}\left|A_{2/3}\right|+\frac{3}{3}\left|A_{3/3}\right|}{\left|A_{1/3}\right|+\left|A_{2/3}\right|+\left|A_{3/3}\right|} \tag{1}$$

where the symbol $|\cdot|$ stands for the cardinality of frequency set. Taking into account that $|A|=|A_{1/3}|+|A_{2/3}|+|A_{3/3}|$, the following relation is obtained:

$$|A|=|u_0|+3|u_1|+3|u_4| \tag{2}$$

Combining Eq.(1) and Eq.(2), the FRF is computed as:

$$\eta=\frac{|u_0|}{|A|}+\frac{1}{3}\times\frac{|u_1|}{|A|}\times 3+\frac{2}{3}\times\frac{|u_2|}{|A|}\times 3 \tag{3}$$

From Eq.(2), we can get the equation about u_1 as follows:

$$|u_1|=\frac{|A|-3\times|u_4|-|u_0|}{3} \tag{4}$$

Following the example of Cell 1, the number of available frequencies in cell-centre is $|u_0|$, whereas in the cell-edge is $|u_1|+2|u_4|$. Assuming that $|u_0|=k(|u_1|+2|u_4|)$, where k is a constant parameter, so $|u_4|$ can be got from Eq.(4):

$$|u_4|=\frac{|u_0|}{3k}-\frac{|u_0|}{9}-\frac{|A|}{4} \tag{5}$$

Finally, taking into account Eq.(4) and Eq.(5), Eq.(3) can be expressed in terms of $|u_0|$:

$$\eta=\frac{1}{12}+\left(\frac{1}{3k}+\frac{5}{9}\right)\frac{|u_0|}{|A|} \tag{6}$$

It can be seen from Eq.(6) that as FRF grows, the available frequency resources in cell-centre increase, while those in cell-edge decrease. Moreover, the performance of the SFR scheme is compared with 3GPP LTE simulation parameters and the SFFR scheme.

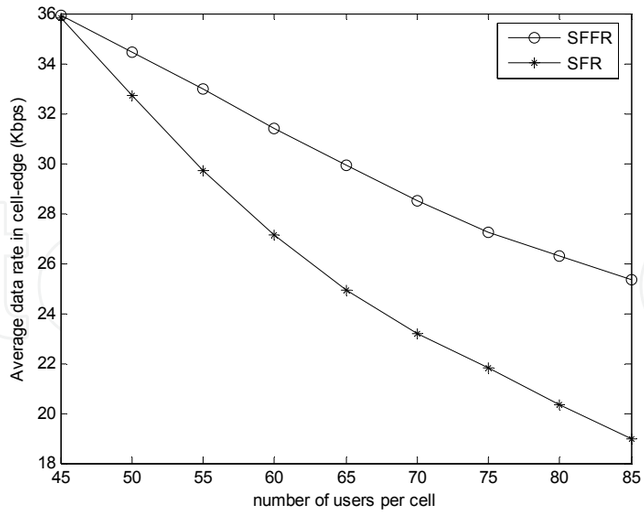


Fig. 2. Comparison of average data rate in cell-edge

Fig. 2 compares the average data rate in cell-edge for SFR and SFFR, where the FRF is set as 8/9. It can be seen that the average data rate in cell-edge decreases as the number of users per cell increases. However, the SFFR scheme outperforms the SFR scheme for a given number of users per cell. Specially, as the increase of users, the improvement by the SFFR scheme is more than that of the SFR scheme, which shows it's more effective when the number of users is large.

In order to mitigate inter-cell interference, a novel inter-cell interference coordination scheme called SFFR is introduced in this part, which can effectively improve the data rate in cell-edge. The numerical results show that compared with the SFR scheme, the SFFR scheme improves the performance in cell-edge.

2.2 Cooperative frequency reuse

In 3GPP LTE-Advanced systems, Coordinated Multi-Point (CoMP) transmission is proposed as a key technique to further improve the cell-edge performance in May 2008. CoMP technique implies dynamic coordination among multiple geographically separated transmission points, which involves two schemes.

a. Coordinated scheduling and/or beamforming, where data to a single UE is instantaneously transmitted from one of the transmission points, and scheduling decisions are coordinated to control.
b. Joint processing/transmission, where data to a single UE is simultaneously transmitted from multiple transmission points.

With these CoMP schemes, especially for CoMP joint transmission scheme, efficient frequency reuse schemes need to be designed to support joint radio resource management among coordinate cells. However, based on the above analysis, most of the existing frequency reuse schemes can not incorporate well with CoMP system due to not considerate multi-cell joint transmission scenario in their frequency plan rule.

In order to support CoMP joint transmission, a novel frequency reuse scheme named cooperative frequency reuse (CFR) will be introduced in this part. The cell-edge areas of each cell in CFR scheme is divided into two types of zones. Moreover, a frequency plan rule

is defined, so as to support CoMP joint transmission among neighbouring cells with the same frequency resources. Compared with the SFR scheme, the simulation results demonstrate that the CFR scheme yields higher average throughput in both cell-edge and cell-average points of view with lower blocking probability.

2.2.1 System model

A typical system model for downlink CoMP joint transmission is described in Fig. 3. In the system, cell users are divided into two classes, namely cell-centre users (CCUs) and cell-edge users (CEUs). We assume only CEUs can be configured to work under CoMP mode. Each CEU has a CoMP Cooperating Set (CCS) formed by the cells that provide data transmission service to this CEU, and the serving cell of each CUE is always included in its CCS. The CEU with more than one cell in its CCS is regarded as a CoMP CEU, which can be served by the cells contained in its CCS simultaneously with the same frequency resources. It is assumed that each cell is configured with one transmitting antenna with one receiving antenna for each user.

As shown in Fig. 3, Cell 1, Cell 2 and Cell3 are formed a CCS for user 1. So user 1 is regarded as a CoMP CEU, and can be served by all these three cells simultaneously with the same frequency resources. Since user 2 is not work under CoMP mode, it can only communicate with its serving cell, i.e. Cell 1.

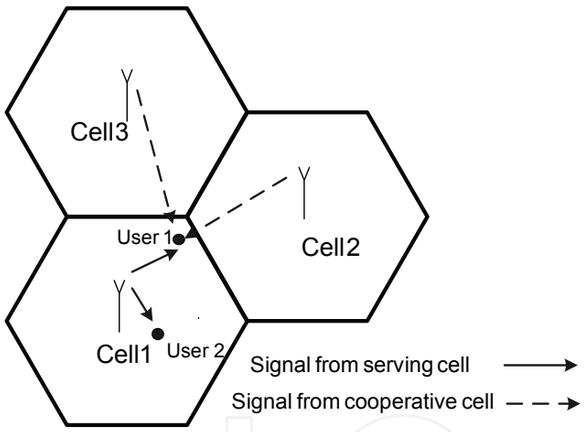


Fig. 3. System Model for downlink CoMP joint transmission

Let Ψ_k denote the CCS of the k^{th} CoMP CEU, Ω denote the overall cells in the system, and $\left\{\Omega \cap \bar{\Psi}_k\right\}$ denote the cells in set Ω while not in set Ψ_k. Therefore, the signal to interference plus noise ratio (SINR) on l^{th} physical resource block (PRB) for k^{th} active CoMP CEU connected to i^{th} cell is determined as follows:

$$\gamma_{i,l}^{k} = \frac{\sum_{s\in\Psi} P_{s,l} G_s^k \left|h_{s,l}^k\right|^2}{N_0 + \sum_{n\in\left\{\Omega\cap\bar{\Psi}_k\right\}} x_{n,l} P_{n,l} G_n^k} \tag{7}$$

Where $P_{s,l}$ is the transmission power from s^{th} cell on l^{th} PRB. For simplicity, $P_{s,l}$ is constant assuming no power control. G_s^k is the long term gain between s^{th} cell and the k^{th} CoMP CEU, consisting of propagation path loss and the shadow fading. $h_{s,l}^k$ denotes the fast fad gain on

l^{th} PRB for the channel between s^{th} cell and k^{th} CoMP UE. N_0 is the noise power received within each PRB. And $x_{n,l}$ is the allocation indicator of l^{th} PRB, which can be given by:

$$x_{n,l} = \begin{cases} 1, & if\ l^{th}\ PRB\ is\ used\ in\ n^{th}\ cell \\ 0, & otherwise \end{cases} \tag{8}$$

In 3GPP LTE standards, it was pointed out that interference coordination is handled by the system once every 100ms. The information reported by the users and used by the system is the average SINR value. Thus, $\left|h_{s,l}^{k}\right|^2$ is replaced by its mean value $E\left(\left|h_{s,l}^{k}\right|^2\right)=1$, and Eq. (7) can be expressed as

$$\gamma_{i,l}^{k} = \frac{\sum_{s\in\Psi_k} P_{s,l}G_s^k}{N_0 + \sum_{n\in\{\Omega\cap\bar{\Psi}_k\}} x_{n,l}P_{n,l}G_n^k} \tag{9}$$

For the users who don't work under CoMP mode, they only communicate with their serving cells. The average SINR on l^{th} PRB for k^{th} user of i^{th} cell is then given by:

$$\gamma_{i,l}^{k} = \frac{P_{i,l}G_i^k}{N_0 + \sum_{n\in\Omega,n\neq i} x_{n,l}P_{n,l}G_n^k} \tag{10}$$

Finally, according to Shannon theorem, the corresponding capacity to the user average SINR on l^{th} PRB can be expressed as:

$$C_{i,l}^{k} = B\log_2\left(1+\frac{\gamma_{i,l}^{k}}{\Gamma}\right) \tag{11}$$

Where B is the bandwidth of each PRB, and Γ called SINR gap is a constant related to the target BER, with $\Gamma = -\ln(5BER)/1.5$.

2.2.2 Cooperative frequency reuse scheme

The principle of the CFR scheme that can support CoMP joint transmission will be introduced here. Each three neighbouring cells are formed as a cell cluster and respectively marked with cell 1, cell 2 and cell 3. The cell-edge area of each cell is then divided into six cell-edge zones according to the six different neighbouring cells. Given the marker of each neighbouring cell, the six cell-edge zones in a cell are then categorized into two types. Hence, there are total six types of cell-edge zones in a cell cluster. As illustrated in Fig.4, each cell-edge zone is marked with A_i^j, where i denotes the cell to which the zone belongs, j is the marker of the dominant interference cell of this zone, note that $i,j=\{1,2,3\}$ and $i\neq j$. For simplifying expression, we just take the cell-edge zones in cell 1 into count:

Zone A_1^2: It is the cell-edge zone of the cells marked with cell 1. Moreover, the dominant interferer of the users in this zone is the nearest neighbouring cell marked with cell 2.

Zone A_1^3: It belongs to the cells marked with cell 1. And the dominant interferer is the nearest neighbouring cell marked with cell 3.

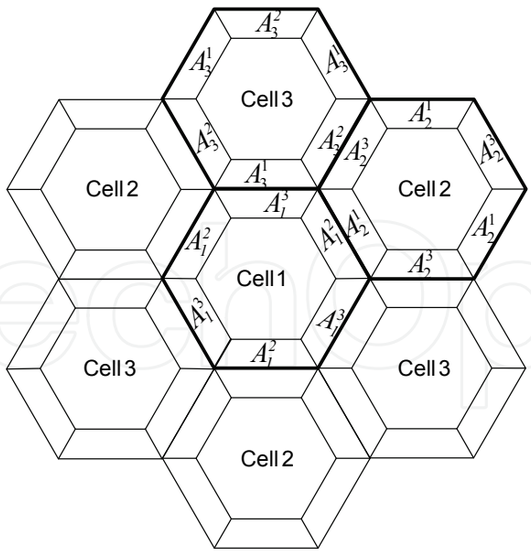


Fig. 4. Cell-edge areas partition for each cell

In order to support multi-cell joint transmission with neighbouring cells, a cooperative frequency subset is defined for each cell in CFR scheme. Then the resources are allocated to users in each cell cluster according to the following frequency reuse rule:

Step1. In each cell, the whole resources are divided into two sets, G and F, where $G \bigcap F = \varnothing$. Resources in set G are used for CCUs in each cell. While resources in set F are used for CEUs.

Step2. Set F is further divided into three subsets, marked by F_1, F_2, F_3, with $F_i \bigcap F_j = \varnothing (i \neq j)$.

Step3. For each cell cluster, F_i is assigned for cell i as a cooperative frequency subset, which is used for providing cooperative data transmission for the CEUs in neighbouring cells.

Step4. F_j is assigned for the CEUs in cell-edge zones marked with A_i^j.

Based on the above mentioned frequency reuse rule, the frequency allocation for a cell cluster is shown in Fig. 5.

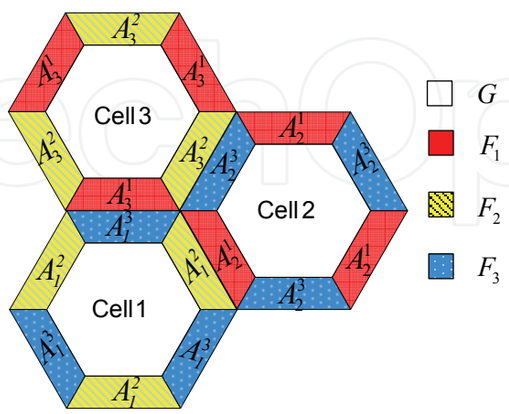


Fig. 5. Frequency assignment for the boundary areas of each cell cluster

On the one hand, orthogonal frequency subsets are allocated to the adjacent cell-edge zones that belong to different cells. Hence, the ICI can be reduced by using different frequency

resources in adjacent areas of neighbouring cells. On the other hand, according to the frequency reuse rule, F_j is allocated for cell-edge zone A_i^j. Besides, it is the cooperative frequency subset for cell j, which is the dominant interference cell of zone A_i^j. Hence, for a CoMP CEU located in zone A_i^j, cell i and cell j can form a CCS. And then provide CoMP joint transmission for this CEU simultaneously with the same frequency resources selected from F_j.

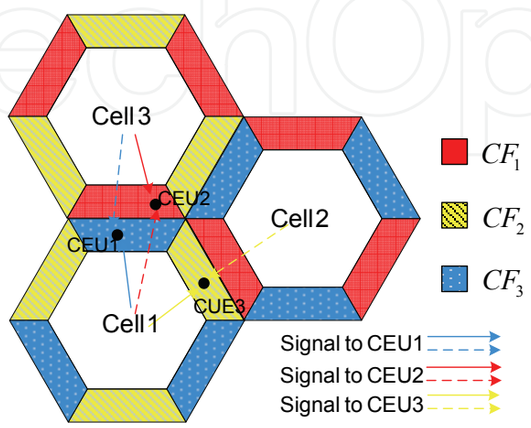


Fig. 6. CoMP joint transmission in CFR system

As shown in Fig.6, when CEU 1 in zone A_1^3 is regarded as a CoMP CEU, its dominant interference cell marked with cell 3 and the serving cell marked with cell 1 can form a CCS. Then CEU 1 can be served by these two cells with the same frequency resources selected from set F_3. What's more, we can see that the whole frequency resources could be reused in all cells. Hence, the frequency reuse factor in CFR scheme can achieve to 1. In CCS selection, we introduce an algorithm for the CCS selection. Let N denote the total number of cells in the system, M denote the maximum number of cells in a CCS of a CEU. The k^{th} CEU's CCS, denoted as Ψ_k, can then be selected according to the user's long term gain G_k^i as follows:

Algorithm: CCS Selection

① $\Psi_k \leftarrow \varnothing$, $count \leftarrow 0$.

② Calculate the long term gain G_k^i between k^{th} CEU and i^{th} cell, for $i = 0,...,N-1$.

$G \leftarrow \left\{G_k^0, G_k^1, ..., G_k^{N-1}\right\}$

③ Find serving cell for k^{th} CEU

$i \leftarrow \arg\max\left(G_k^i\right), G_k^i \in G$

$s \leftarrow i$

④ Update

$\Psi_k \leftarrow \Psi_k \bigcup \left\{i^{th}\ cell\right\}$

$count \leftarrow count + 1$

⑤ If $count < M$,
$G \leftarrow G - \left\{G_k^i\right\}$
$i \leftarrow \arg\max\left(G_k^i\right), G_k^i \in G$
Else stop.
⑥ If $G_k^s - G_k^i \le thr$, go to ④
Else stop.

It has been proved that the maximum size of UE-specific CoMP cooperating set equal to 2 is enough to achieve CoMP gain for 3GPP case 1 in references. Hence, the value of M is set to 2 in this paper. CEUs with two cells in their CCS are regarded as CoMP CEUs, whose SINR can be improved by CoMP joint transmission with the same frequency resources according to the introduced frequency reuse rule.

2.2.3 Performance analysis

System level simulations are performed to evaluate the performance of the introduced CFR scheme. As performance metrics, we used the blocking probability and the average throughput in both the cell-edge and cell-average points of view. The universal frequency reuse (UFR) where PRBs are randomly assigned to the different users in each cell irrespective of their category (CEU or CCU) is taken as a reference scheme. Another reference scheme is SFR scheme, which assigns a fixed non-overlapping cell edge bandwidth to a cluster of three adjacent cells. For the introduced CFR scheme, two cases are studied, where Thr is 0 dB and 5 dB respectively.

We focus on an OFDMA-based downlink cellular system. A number of UEs are uniformly dropped within each cell. The basic resource element considered in the system is the PRB, which consist of 12 contiguous subcarriers. It is assumed that all the available PRBs are transmitted with equivalent power. Only one PRB can be assigned to each active UE. The main simulation parameters listed in Table.1 are based on 3GPP standards.

Parameters	Values
Carrier Frequency	2 GHz
Bandwidth	10 MHz
Subcarrier spacing	15 kHz
Number of subcarriers	600
Number of PRBs	50
The number of cells	21
Cell radius	500m
Maximum power in BS	46 dBm
Distance-dependent path loss	L=128.1+37.6log10 d (dB), d in km
Shadowing factor variance	8dB
Shadowing correlation distance	50m
Inter cell shadow correlation	0.5

Table 1. Simulation Parameters

Fig. 7 shows the blocking probability of the introduced CFR scheme and the conventional SFR scheme as a function of the loading factor. We can see that CFR scheme performs quite better than the SFR scheme. Specially, the blocking probability reduced by SFR scheme is 50% more than SFR scheme. For example, if it is required that the blocking probability must not exceed 5%, Fig.7 indicates that the admissible loading factor of the SFR scheme is only 30%, while the admissible loading factor of the introduced CFR scheme is more than 60% of the total frequency resource. This improvement in the CFR scheme results from the frequency reuse rule designed for each cell cluster. According to the frequency reuse rule, the number of available frequency resources for the cell-edge areas of each cell is twice as great as the conventional SFR scheme.

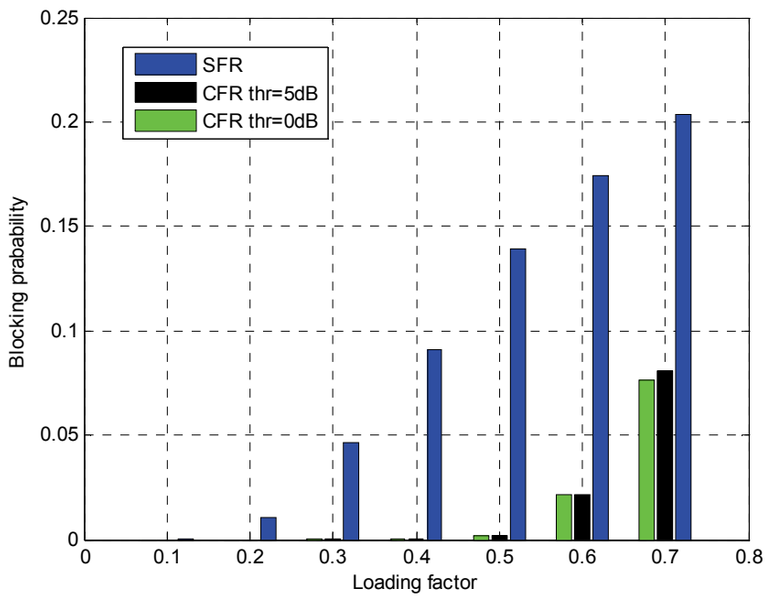


Fig. 7. Blocking probability as a function of the loading factor

Fig. 8 shows the cell-edge average throughput per user for the three different frequency reuse schemes considered in this paper. It can be seen that the average throughput per CEU decreases as the number of users increases in all the three schemes. That is because the probability of PRBs collision increases as the number of users grows. In other words, the ICI increases when the average number of users per cell grows. Moreover, compared with UFR scheme, both CFR scheme and SFR scheme yield a significant improvement in terms of cell-edge average throughput owing to the frequency reuse plans for cell-edge areas.

We can also observe that the introduced CFR scheme achieves higher cell-edge average throughput than SFR scheme. When *Thr* is 0 dB, no user works under CoMP mode. Compared with SFR scheme, the cell-edge average throughput is improved by 4 to 8%, which is achieved mainly owing to the frequency reuse rule designed in CFR scheme. When *Thr* is set to 5dB, the throughput raised by the introduced CFR scheme is 30 to 40% more than the SFR scheme, that is because part of the CEUs are regarded as CoMP users whose throughput can be further improved by CoMP joint transmission.

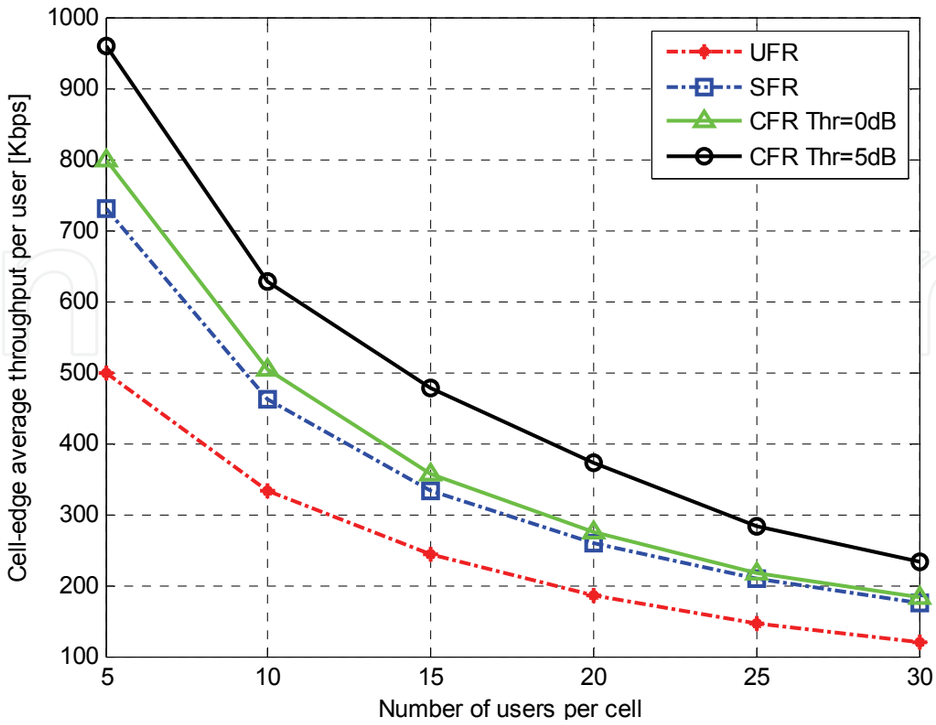


Fig. 8. Cell-edge average throughput per user

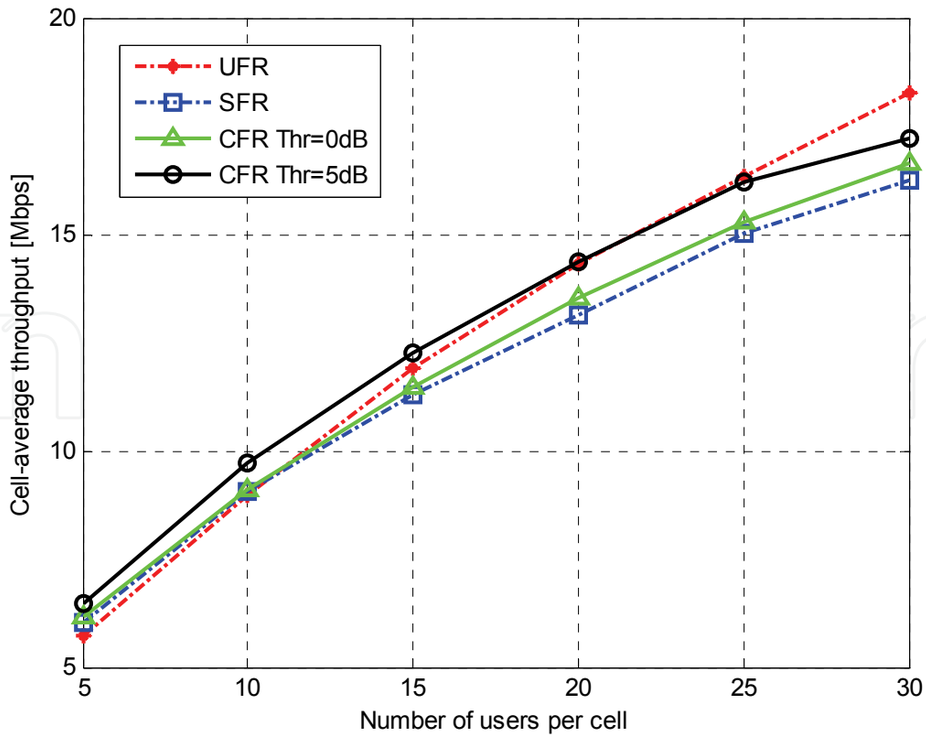


Fig. 9. Cell-average throughput as a function of the number of users per cell

Fig. 9 shows the cell-average throughput of the introduced CFR scheme and the two conventional frequency reuse schemes as a function of the number of users per cell. From the graph, we can see that the cell-average throughput of the introduced CFR scheme outperforms that of the SFR scheme due to better cell-edge performance and lower blocking probability. When *Thr* is set to 0dB, the cell-average throughput is improved by 1 to 3%. While when *Thr* is set to 5dB, the cell-average throughput is improved by 5 to 9%.

It is also can be seen that when the number of users per cell is small, i.e. less than 15, CFR scheme with *Thr* equals to 5dB achieves the best results among the three schemes under consideration. When the number of users is large, UFR scheme achieves the better results than the introduced CFR scheme. However, the payoff for this higher average cell throughput of UFR scheme is a huge decrease in cell-edge average throughput which can be observed from Fig. 8.

2.2.4 Summary

In this part, a novel frequency reuse scheme named CFR is introduced to support CoMP joint transmission and further improve cell-edge performance. First, the method for cell-edge areas partition is introduced, which divides the cell-edge areas of each cell into two types of zones. Then, the frequency plan rule is defined for each cell cluster, which assigns a cooperative frequency subset for each cell and makes CoMP users in cell-edge zones can be served by multi-cell joint transmission with the same frequency resources. In addition, the algorithm is given for the CEUs to select cells in their CCS. The simulation results demonstrate that the introduced CFR scheme significantly outperforms the conventional SFR scheme in terms of blocking probability, cell-edge average throughput and cell-average throughputs.

3. Inter-cell interference prediction

In order to mitigate the inter-cell interference in OFDMA systems, three schemes are given in 3GPP organization, which respectively are interference coordination, interference cancellation and interference randomization. However, the traditional inter-cell interference mitigation schemes belong to passive interference suppression measures, and its effectiveness is still limited. Considering this situation, an active interference mitigation strategy will be introduced in this part, named as interference prediction. By means of the immediate interference prediction in cell, it enables to efficiently avoid and eliminate inter-cell interference, which is a novel type of active interference mitigation strategy.

For interference prediction, this part takes use of the optimal estimation theory. Generally, the problems about optimal estimation theory can be classified into three categories: The first is the model parameter estimation problem, such as the least squares method. The second is time series and optimal filtering estimates problem (the optimal estimation of signal or state). The third is the optimal information fusion estimation. According to the actual situation in inter-cell interference prediction, the second problem of optimal estimation is focused.

The inter-cell interference prediction principle is based on optimal estimation theory, forecasting the co-frequency interference in the next timeslot by means of the former or current channel state, and making the mean square error to be the smallest. The optimal estimation theory includes time-series estimation, optimal filtering estimation method, etc.

Especially, the optimal filtering estimation aims to estimate the signal state, including several filtering estimation algorithms, such as Wiener filter, Kalman filter, and so on.

3.1 Time series

In time series analysis, it aims to establish the time series model, predict and control signal change state based on such model. Moreover, we define the observation sequence as $\{z_t | z_1, z_2, \cdots, z_n, \cdots\}$, the linear mixed coefficient as $\{a_t | a_1, a_2, \cdots, a_n, \cdots\}$, then the future value $\{z_{t+k} | k > 0\}$ can be predicted by means of current and past time series records $\{z_t, z_{t-1}, z_{t-2}, \cdots\}$. The predicted value is written as $\hat{z}_{t+k|t}$, which meets following condition:

$$\hat{z}_{t+k|t} = \sum_{i=0}^{\infty} a_i z_{t-i} \tag{12}$$

The optimal predicted value $\hat{z}_{t+k|t}$ should make the mean square error be minimum, which should obey

$$Min\left\{E\left[\left(\hat{z}_{t+k|t} - z_{t+k}\right)^2\right]\right\} \tag{13}$$

In the above theoretical derivation, the present and past observed records $\{z_t, z_{t-1}, z_{t-2}, \cdots\}$ belong to be infinite series, which is difficult to achieve in practice. Considering this situation, the finite time series of recursive predictor are introduced, such as Box-Jenkins method, Astrom method, etc. Besides, the steps of Box-Jenkins method are as follows:

a. For the observed sequence $\{z_t | t = 1, 2, \cdots, N\}$, calculate its correlation coefficient and partial autocorrelation coefficient, then test whether the sequence is non-stationary white noise sequence. If such sequence is white noise series, go to the end. If such sequence is non-stationary series, take model according to non-stationary time series principle. Else if the sequence is stationary series, take zero for the mean of such sequence and then make model by the Box-Jenkins method.
b. Test the type of zero mean stationary series. Illustrately, determine the series $\{z_t | t = 1, 2, \cdots, N\}$ belong to which model, such as autoregressive (AR) model, moving average (MA) model and autoregressive moving average (ARMA) model.
c. After the model is identified, judge the highest level of such model, and make fitted test from low level to high level. For example, if $\{z_t | t = 1, 2, \cdots, N\}$ belong to AR model, make use of $AR(n, n-1)$, and then the fitted test.
d. Compare with different models and find the right model. On this basis, respectively take adaptive test and error test for the initial model, and select the optimal model.
e. Make prediction by the established model.

3.2 Optimal filter estimation

The nature of filtering is the statistical estimation problem. For example, linear minimum variance estimation methods try to make the variance of estimated value and the actual value minimum. Moreover, such filter is also known as the optimal filter, such as Wiener filter and Kalman filter. The interference prediction process by Kalman filter is shown respectively in Fig. 10 and Fig. 11.

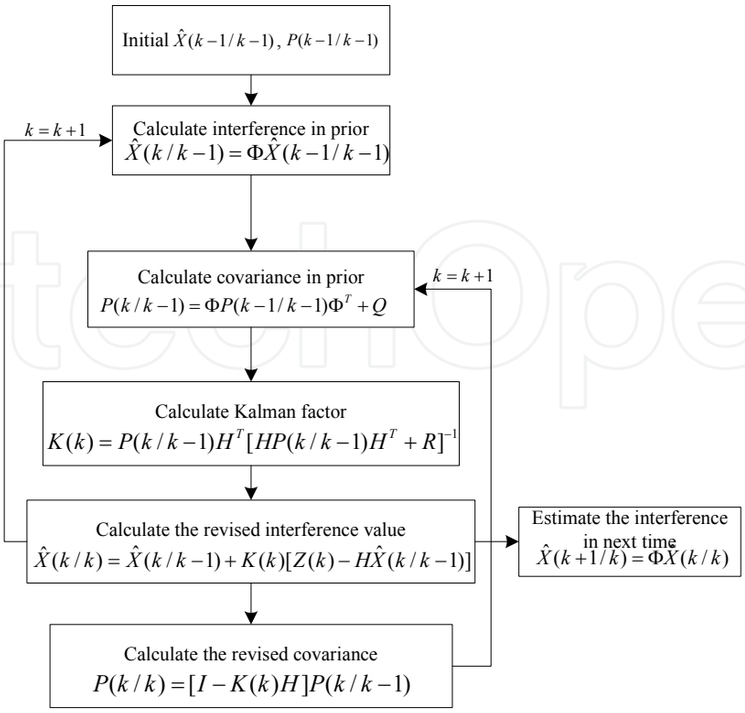


Fig. 10. Interference prediction by Kalman filter

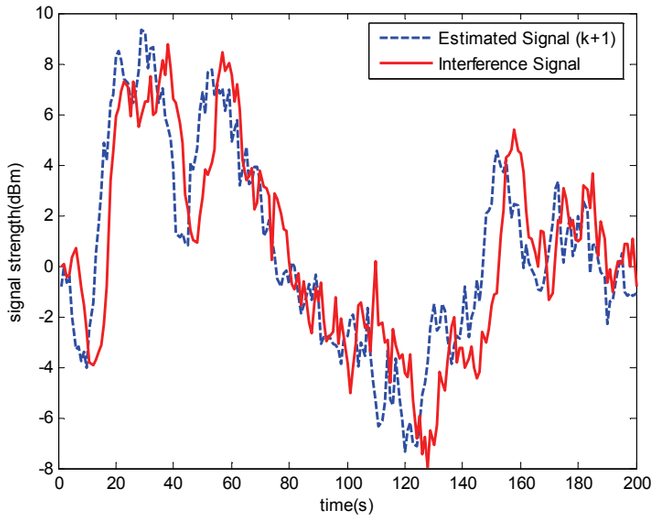


Fig. 11. Interference prediction results by Kalman filter

3.3 Effectiveness principles

The effectiveness of channel prediction criteria was analyzed and the relationship with the predicted time delay and the prediction accuracy of SINR are described in the reference. According to the wireless signal propagation, the mobility rate is closely related with the signal coherence time. If user's mobility rate increases, the coherence time becomes shorter.

Else user's mobility rate decreases, the coherence time becomes longer. The relationship of coherence time and the predicted delay time are divided into three categories, respectively $\tau \gg \Delta t$, $\tau \cong \Delta t$ and $\tau \ll \Delta t$.

Fig.12 shows the prediction results when the coherence time is much greater than the time delay, which is that $\tau \gg \Delta t$. At this time, user is in a slow moving state, and the channel state information (CSI) can be easily obtained. From Fig.12, we can see the predicted SINR in delay time approximates to the actual value.

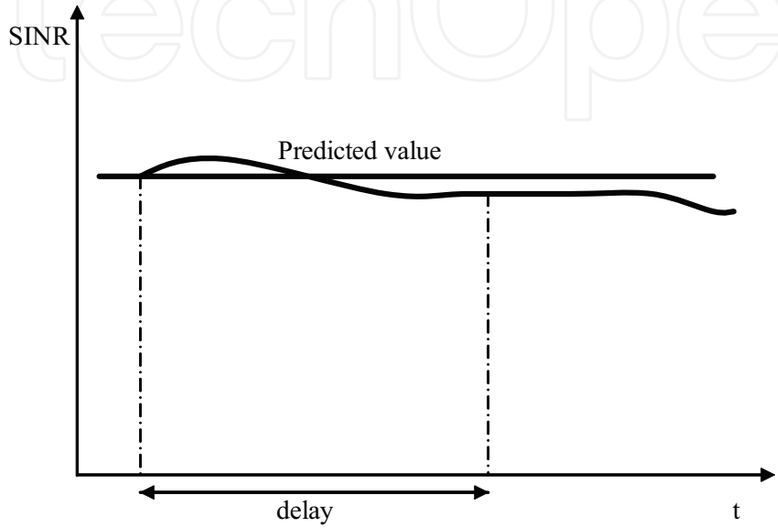


Fig. 12. SINR prediction ($\tau \gg \Delta t$)

Fig.13 shows the prediction results when the coherence time approaches to the time delay, which is that $\tau \cong \Delta t$. At this time, user's moving speed is in a medium state. In order to ensure the continuity of information transmission, the SINR should obey the outage criteria and keep a conservative prediction, which is the threshold SINR value.

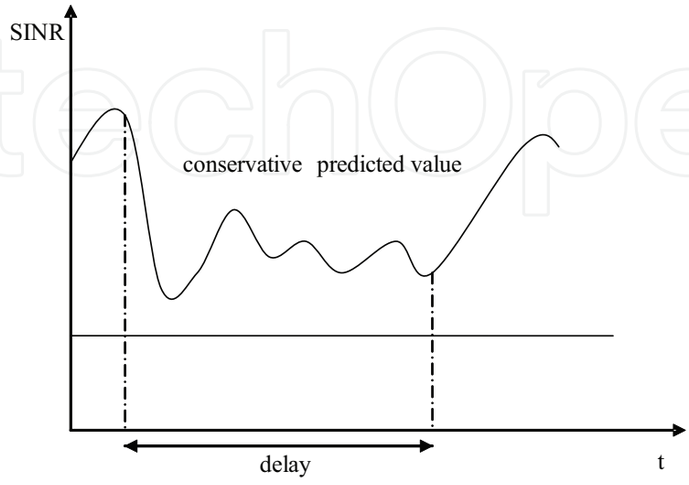


Fig. 13. SINR prediction ($\tau \cong \Delta t$)

Fig. 14 shows the prediction results when the coherence time is far less than the time delay, which is that $\tau \ll \Delta t$. At this time, user's rate is in a high speed state, the coherence time is shorter and the CSI is hard to be obtained. In this situation, we only need to predict the average SINR.

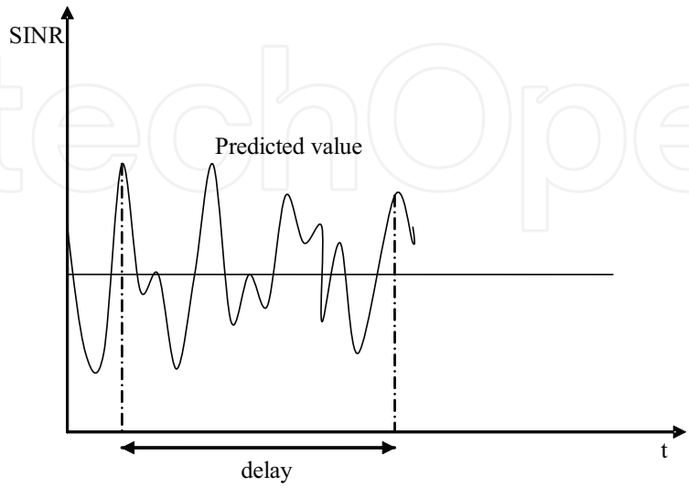


Fig. 14. SINR prediction ($\tau \ll \Delta t$)

3.4 Summary

In this part, the inter-cell interference prediction is introduced, which is an active interference mitigation method. The theoretical basis, which is the optimal estimation theory, is provided with including of two parts: time series and the optimal filter estimation. Besides, the reliability is also analyzed by means of prediction accuracy, which is based on the relationship of the coherent time and the time delay. In addition, the trend for the actual measured radio signals is analyzed with AR model, MA model and ARIMA model. The analytical results are provided to show time series model can efficiently predict the radio signals change and then mitigate the interference effectively.

4. Inter-cell interference cancellation

Inter-cell interference cancellation strategy aims at interference suppression at the user equipments by improving the processing gain. In order to solve this problem, two basic schemes have been discussed in 3GPP proposals. One is to take spatial suppression at the UE side by means of multiple antennas; the other is to directly detect and subtract the inter-cell interference in order to enable inter-cell-interference cancellation. Usually, the inter-cell interference cancellation strategy is used to get the processing gain through suppress strong interference. According to the degree of knowledge available about interferers, interference cancellation methods can be distinguished as three categories, which are blind, semi-blind, and full-knowledge.

Many inter-cell interference cancellation methods are based on generalized spatial diversity. Beam forming is introduced in inter-cell interference cancellation in references. By distinguish different users in space, it effectively reduces interference among users. But on

the other hand, it brings with extra interference from main lobe and strong side lobe. A method of subcarrier-based virtual MIMO in inter-cell interference cancellation was proposed, which is introduced in OFDM-based systems with a frequency reuse factor equal to 1. But when UE is located between sectors, inter-sector interference cannot be reduced by the subcarrier-based virtual MIMO (SV-MIMO) due to loss of channel separability. Inter-cell interference cancellation by virtual smart antennas was also studied, which proposes a method for estimating inter-cell symbol timing offsets using multiple signal classification (MUSIC) algorithm. For the use of MUSIC algorithm, the premise is to know the number of source. But in practice, the number of source can not be accurately obtained, which may make MUSIC algorithm not work. Moreover, in most case, many similar algorithm needs to know current channel state information, but at the same time, the complexity of system may be increased if acquire it in downlink. As a result, how to mitigate inter-cell interference in no precise channel is an important problem.

In order to effectively mitigate inter-cell interference in OFDM-based systems, this part focuses on the inter-cell interference cancellation strategy. A novel inter-cell interference mitigation method for OFDM-based cellular systems will be introduced. Compared to the existing methods, the independent component analysis based on blind source separation is presented in inter-cell interference, and the signal to interference plus noise (SINR) is set up as the objective function. This scheme can adapt to the no precise channel conditions, and can mitigate inter-cell interference in a semi-blind state of source signal and channel information.

4.1 Inter-cell interference model

Considering the downlink in cell-edge, assume this MIMO system with q transmission antennas in the serving eNodeB, and p receiving antennas in UE. In such scenario, UE not only receives useful signal from current communicating base station, but also receives noise and interference from other adjacent base stations. The example is shown in Fig. 15.

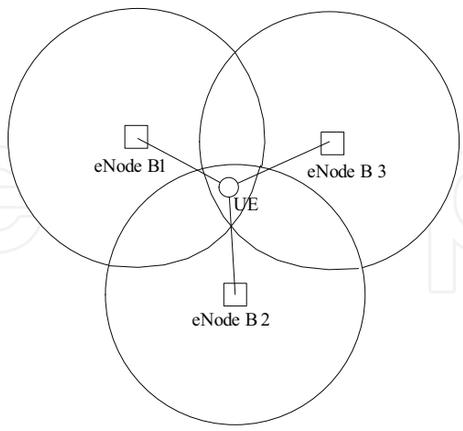


Fig. 15. Inter-cell interference in cell-edge

For many OFDM-based systems, the original signal is transmitted from OFDM transmitter and through MIMO antenna array. The process of inter-cell interference mitigation is shown in Fig.16. Further, we assume the original signal interfered by inter-cell interference and thermal noise, and the channel information is unknown.

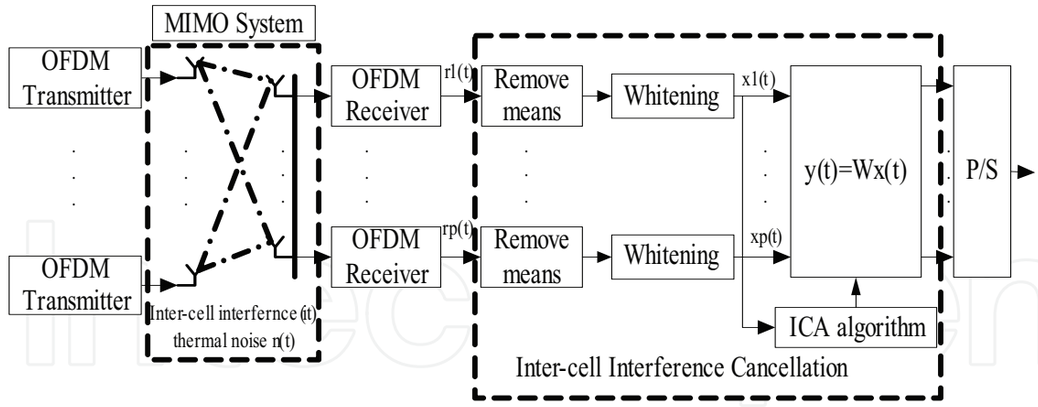


Fig. 16. Inter-cell interference mitigation process

According to the principle in radio signal propagation, the thermal noise can be seen as independent with transmission signals from eNodeB. Compared to the inter-cell interference from other cells, we assume the useful signal is statistically independent with the co-frequency interference from other different cells. So it can be thought that useful signal, unknown inter-cell interference and thermal noises are statistically independent and irrelevant with each other. Moreover, some parameters are defined as follows:

$s(t) = \{u(t), i_1(t), ..., i_k(t), ..., i_{n-2}(t), n(t)\}$ denotes as the source signal, which is constructed by the useful signal, inter-cell interference and the thermal noise, also written as $(s_1, s_2, ..., s_n)^T$. Specifically, $u(t)$ denotes as the useful signal. $i_k(t)$ denotes as the kth unknown additive inter-cell interference with the same frequency, which is in the range of 1 to $n-2$. The dimension for the number of eNodeB reused with the co-frequency subcarriers is $n-2$. $n(t)$ denotes as the additive zero mean thermal noise, also the Gaussian noise.

At the receiving end, we denote $r(t)$ as the received signal, mixed with the useful signal, unknown additive interference and noise. α, β_k and γ are respectively the mixing vectors. So $r(t)$ can be written as the following equation:

$$r(t) = \alpha u(t) + \sum_{k=1}^{n-2} \beta_k i_k(t) + \gamma n(t) \tag{14}$$

Furthermore, Let A denote as linear mixing matrix, which reflects temporal radio signals transmission process and all interference from other adjacent cells are linear mixture. Then the inter-cell interference model can be written as:

$$r(t) = As(t) \tag{15}$$

From Eq.(15), it can been seen that the dimension of $r(t)$ is the same to $s(t)$, which is equal to n. In order to separate the useful signal from inter-cell interference and thermal noise, we take interference cancellation by independent component analysis (ICA), which is an important method in blind source separation (BSS). As shown in Fig.16, we deal with the received signal by remove means and whitening, and such process is set as the transition matrix V. So we can get:

$$x(t) = Vr(t) \tag{16}$$

On the other side, we set up a separation matrix W, and make $WVA = I$ in theory. Moreover, assume $y(t)$ is the separated signal after removing interference and noise, so $y(t)$ can be got by following equation:

$$y(t) = Wx(t) = WVAs(t) = Gs(t) \tag{17}$$

But in fact, because exist with errors and uncertainties, we need to get an optimal approximate solution that can make such a separation matrix W approach to the condition $G = I$. By means of ICA methods, an objective function is established, which takes W as a variable function. When W takes some value, the objective function can achieve to minimum or maximum. At this moment, the variable W is the optimal approximate solution.

4.2 Independent component analysis

In many fields, it needs to separate all the source signals from the mixed signals with no precise knowledge of the source signals and the channel information, whose processes are usually called as blind source separation (BSS). In order to solve such problem, many schemes have been researched. When the source signals are not independent with each other in BSS, some separating schemes are introduced, such as sparse component analysis (SCA), smooth component analysis (SMOCA), non-negative matrix factorization (NMF), and so on. However, the complexity of such algorithms is still high and hard to realize in application.

On the other hand, when the source signals are independent with each other in BSS, the independent component analysis (ICA) schemes are proposed. By principle of independence, the separating complexity is reduced and the results are also improved. Specially, some methods exist in ICA, such as Informax, Fast ICA, generalized eigenvalue decomposition, etc. Informax algorithm is proposed by Bell, whose characteristic is searching for the maximum mutual information between the received signal and the output signal, but its convergence is always slowly. Fast ICA is a fast and fixed-point algorithm proposed by A. Hyvrinen, whose characteristic is computing the maximum kurtosis by iterations. Although its convergence is improved compared with Informax, the effects of thermal noise are always not included in iterations. The ICA based on generalized eigenvalue decomposition is proposed by L. Parra, whose characteristic is decomposing generalized eigenvalue for the received signal. However, this method is limited by the type of source signals.

The critical step in ICA process is to make the estimated independent component gradually approach to the source signal by means of establishing objective function and finding its optimal solution.

According to the classical formula dealing with ICA problems, some requirements must be made in the known conditions in order to get definite solution, as follows:

a. The source signals are all real random signals, and the respective mean is zero. Moreover, these signals are statistically independent with each other.
b. There is at most one source signal whose probability density characteristic is the Gaussian distribution, while the other source signals obey non-Gaussian probability distribution.
c. For the source signals, the approximate probability distribution functions (PDF) need to be acquired.

d. The number of source signals and received signals is equal, and the mixing matrix A is a square matrix.

But in inter-cell interference cancellation, we only need to separate the useful transmission signals from the inter-cell interference and noise, which means we don't need to separate all source signals from the mixed signals. Specially, we can take use of some identity of the useful signals in this situation, such as training sequence.

Based on the above analysis, and in order to verify the inter-cell interference cancellation scheme by ICA methods, some conditions need to be illustrated as follows:

a. Considering the offset of carrier frequency and phase, it may bring with some intra-cell interference actually. In analysis, we neglect such interference, but only consider the inter-cell interference and thermal noise. Moreover, the inter-cell inferences from different cells are seen as statistically independent with each other, and all these signals are linear mixed.
b. By the principle of BSS, the means of the received signal from different eNodeB can be respectively conversion into zero by the process of removing means, and such signals can also be changed into real random signals by whitening, as shown in Fig.16.
c. According to the experienced formulas, the voice signals are usually with Super-Gaussian distribution, for the kurtosis of such signals is positive. While the image signals are usually with Sub-Gaussian distribution, for the kurtosis of such signals is negative. Among the mixed signals, only thermal noises are with Gaussian distribution, whose kurtosis is zero.
d. Specially, if the strength of inter-cell interference from adjacent eNodeB is much stronger than the useful signal in cell-edge, it may reach the handover threshold and the inter-cell handover process may be triggered. Moreover, we set the handover threshold as -10dB in this paper, without considering ping-pong effects.
e. Because only need to separate partial signals from the mixed signals, not all the signals, we don't require all signals received by UE are included in the mixed signals, which means the number of the source signals and the received signals may be unequal. By generalized matrix theory, generalized eigenvalue and generalized inverse matrix can be computed, so it doesn't restrict that A is a square matrix.

Based on the compared analysis, ICA method is taken into inter-cell interference cancellation for OFDM-based systems. Different from traditional ICA methods in BSS, we only need to separate partial useful signals from the mixed signals, not all the signals. Moreover, the training sequence can be used to identify the useful signal in order to avoid the ambiguity of separated signal, and this process may be in a semi-blind state.

By means of the existing ICA methods, a Max-SINR ICA algorithm is constructed, which considers the effects of both interference and thermal noise, raises the speed of convergence and improves the output SNR.

4.2.1 Establish objective function

Considering the signal to interference plus noise ratio (SINR) is one of important measured parameters in communication systems, we set up SINR as the objective function.

Assume the following system parameters are given when the system is set up: the source signal $s(t)$, the received signal $x(t)$, the separated signal $y(t)$, the interference and noise $e(t) = y(t) - s(t)$, and the weighted coefficient in the ith antenna is defined as ω_i, so the SINR in user equipment can be defined as follows:

$$F(y) = SINR = 10\lg\frac{s(t)\cdot s^T(t)}{e(t)\cdot e^T(t)} = 10\lg\frac{s(t)\cdot s^T(t)}{[y(t)-s(t)]\cdot[y(t)-s(t)]^T} \tag{18}$$

Assume the separated signal in the ith antenna is $y_i(t)$, the number of receiving antenna is p. For $s(t)$ is unknown in the conditions, we take the weighted arithmetic mean $\overline{y}(t)$ in place of $s(t)$ as an unbiased estimation, that is

$$s(t) = \overline{y}(t) = \frac{1}{p}\sum_{i=1}^{p}\omega_i y_i(t) \tag{19}$$

$$F(y) = 10\lg\frac{\overline{y}(t)\cdot\overline{y}^T(t)}{[y(t)-\overline{y}(t)]\cdot[y(t)-\overline{y}(t)]^T} \tag{20}$$

Also as $y(t) = W\cdot x(t)$, $\overline{y}(t) = W\cdot\overline{x}(t)$, where W is the separation matrix, so Eq. (20) can be equal to

$$F(W) = 10\lg\frac{Wx(t)x^T(t)W^T}{W[x(t)-\overline{x}(t)]\cdot[x(t)-\overline{x}(t)]^T W^T} \tag{21}$$

Then, take expectations on $F(W)$, which is

$$G(W) = E\{F(W)\} \tag{22}$$

For $x(t)$, let $C = E\{x(t)x^T(t)\}$ represent the variance matrix, and let $\tilde{C} = E\{[x(t)-\overline{x}(t)]\cdot[x(t)-\overline{x}(t)]^T\}$ represent the covariance matrix, so we can get

$$G(W) = 10\lg\frac{WCW^T}{W\tilde{C}W^T} \tag{23}$$

4.2.2 Optimize initial separation matrix

In order to get the maximum of $G(W)$ about W, take partial derivative in Eq. (10), and let it equate to zero, that is:

$$\frac{\partial G(W)}{\partial W} = 0 \tag{24}$$

Through Eq. (24), we can get an equation about W. By solve this equation, the solution W can be got. According to the proof in Theorem 1, W is the eigenvector of generalized matrix $\tilde{C}^{-1}C$.

Theorem 1: The separation matrix W is the eigenvector of generalized matrix $\tilde{C}^{-1}C$, where $\tilde{C}^{-1}$ is the general inverse matrix of covariance matrix $\tilde{C}$, and C is the variance matrix.

Proof:

By simplify Eq. (24), we can get

$$\frac{2CW}{WCW^T} = \frac{2\tilde{C}W}{W\tilde{C}W^T} \tag{25}$$

Then combined with the known conditions $C = AC_sA^T$, $\tilde{C} = A\tilde{C}_sA^T$ and $WA = I$, Eq. (25) can be simplified as:

$$WCW^T = WAC_sA^TW^T = C_s$$

$$W\tilde{C}W^T = WA\tilde{C}_sA^TW^T = \tilde{C}_s$$

Put the above expressions into Eq. (25), so

$$\frac{CW}{C_s} = \frac{\tilde{C}W}{\tilde{C}_s} \tag{26}$$

$$\Rightarrow CW = (\frac{C_s}{\tilde{C}_s})\tilde{C}W \tag{27}$$

For the source signals $s(t) = (s_1, s_2, ..., s_n)^T$, for $i = 1, ..., n$, and $j = 1, ..., n$, when $i \neq j$, because s_i and s_j are independent and irrelevant, so $E\{s_i s_j^T\} = 0$; only when $i = j$, it's nonzero, and let $b_i = E\{s_i s_i^T\}$, which means the variance. Further, set the covariance as $\tilde{b}_i = E\{[s_i - \overline{s}_i] \cdot [s_i - \overline{s}_i]^T\}$. On this basis, the matrix constructed by variance and covariance is respectively as follows:

$$C_s = E\{s(t) \cdot s^T(t)\} = diag[b_1, ..., b_i, ..., b_n]$$

$$\tilde{C}_s = E\{[s(t) - \overline{s}(t)] \cdot [s(t) - \overline{s}(t)]^T\} = diag[\tilde{b}_1, ..., \tilde{b}_i, ..., \tilde{b}_n]$$

Assume $\lambda_i = \frac{b_i}{\tilde{b}_i}$, by matrix calculating formula, we can get $\frac{C_s}{\tilde{C}_s} = diag[\lambda_1, ..., \lambda_i, ..., \lambda_n]$. Then simplify Eq. (27), as following:

$$\tilde{C}^{-1}C \cdot W = diag[\lambda_1, ..., \lambda_i, ..., \lambda_n] \cdot W \tag{28}$$

As is shown in Eq. (28), W is the eigenvector of generalized matrix $\tilde{C}^{-1}C$. So we can get the separation matrix W by compute the eigenvector of $\tilde{C}^{-1}C$. The proof is the end.

On the other side, the sizes of eigenvalues reflect different signal strength. By Eigenvalue separation, the information about the useful signal can be found among the mixed signals, which enables to optimize the separating process. On this basis, we need to separate partial useful signals from the mixed signals, while remove the inter-cell interference and thermal noise represented by some other eigenvalues.

4.2.3 Max-SINR ICA algorithm

In order to mitigate the inter-cell interference by cancellation, we take SINR as the objective function, making it to the maximum. Based on Fast ICA algorithm in BSS, the steps of this algorithm are introduced as follows:

a. Step1: Remove the mean of the original signals $r(t)$ by filtering.
b. Step2: Perform the data whitening through the equation $x(t) = D^{-1/2}E^T r(t)$, where D is the eigenvalue matrix and E is the eigenvector matrix. Moreover, D and E can be got by the generalized eigenvalue decomposition of the matrix $R = E\{r(t)r^T(t)\}$.
c. Step3: According to the mixed signal $x(t)$, construct the variance matrix and the covariance matrix as: $C = E\{x(t)x^T(t)\}$, $\tilde{C} = E\{[x(t) - \overline{x}(t)] \cdot [x(t) - \overline{x}(t)]^T\}$
d. Step4: Calculate the generalized eigenvalues and generalized eigenvectors by Eq. (29), and find the eigenvalue and its eigenvector $\hat{W}$, which is the initial separation matrix.

$$CW = (\frac{C_s}{\tilde{C}_s})\tilde{C}W \tag{29}$$

e. Step5: Set the initial value $k = 0$, and normalize $\hat{W}$ by the equation $W_0 = \hat{W} / \left\|\hat{W}\right\|$.
f. Step6: Judge whether $\left\|W_k^T W_k\right| - 1\right| \le \varepsilon$, in which ε is arbitrary small. If set up, output W_k; else go to following iterations:
while $k \le k_{\max}$
while $\left\|W_k^T W_k\right| - 1\right| > \varepsilon$
do $W_k = E\{(W_{k-1}^T x)^3 x\} - 3W_{k-1}$
$W_k = W_k - \sum_{i=0}^{k-1} (W_k^T W_i) W_i$
$W_k = W_k / \|W_k\|$
end
$k = k + 1$
end
g. Step7: Separate the useful transmitting signals from the mixed signals.

$$y(t) = Wx(t) \tag{30}$$

4.2.4 Select useful signals

Considering the inter-cell interference from different cells must be with different training sequences, so the useful signals can be selected according to following equation:

$$d_i = \sum_{i=1}^{N_s} \left(\hat{a}_i(t) - a_0^T(t)\right)^2 \tag{31}$$

Where N_s is the length of training sequence constructed by the Gold sequence, $\hat{a}_i(t)$ is the estimated value of training sequence symbol, and $a_0(t)$ is the known value of training sequence symbol.
On the other hand, the estimated training sequence of useful signal and the known training sequence must be with the minimum distance, so it can get

$$d = Min\{d_1, d_2, ..., d_n\} \tag{32}$$

By means of Eq.(32), we can select the useful signal $u(t)$ from the separated signals.

4.3 Performance evaluation

In order to verify the results of such inter-cell interference cancellation method introduced in this paper, the static simulation is performed in the OFDM-based environment. The simulation parameters are described in Table 2, and the process of inter-cell interference cancellation by Max-SINR ICA is shown in Fig.16. In static simulation, we assume the position of each UE is fixed, and neglect the Doppler frequency effect.

Parameters	*Values*
Channel environment	Rayleigh fading
Carrier Frequency	2 GHz
Bandwidth	10 MHz
Distance of sub-carrier	15 kHz
FFT size	1024
No. of subcarriers	512
No.of cells	3
Cell radius	1 km
Modulation	BPSK
Convolutional codes rate	1/2
Symbols per frame	200
Length of symbol	1/20 ms

Table 2. Simulation Parameters

In performance evaluation, some parameters are taken as measurement, such as input SINR, output SNR, average number of iterations, etc. Moreover, we assume the number of signals in the received signal subspace equal to the source signal, and there are only four source signals mixed in linear that respectively from three different eNodeB and the thermal noise. One is the useful transmission signal, while the others are seen as the interference.

By the analysis, we compare the Max-SINR ICA algorithm with the classical Fast ICA algorithm, and the results illustrate that the advantage of the introduced algorithm is obvious. Specifically, the convergence of such two ICA algorithms is compared. Two situations are considered in simulation, which respectively the length of processing frame is fixed and the strength of thermal noise is fixed.

4.3.1 Convergence comparison

In order to compare the convergence of Max-SINR ICA algorithm with other classical ICA algorithms, we take the Fast ICA algorithm as an example, and simulation is performed. The result is shown in Fig. 17, where the average number of iterations is as a function of the input SINR ($SINR_{in}$). The length of processing frame is set as 50 symbols, while the input SNR (SNR_{in}) is set as 40 dB.

From Fig. 17, it can be seen that the convergence speed for the introduced Max-SINR ICA is faster than Fast ICA. With the same value of $SINR_{in}$, the average number of iterations for Max-SINR ICA is less than Fast ICA. Generally, the iteration number is determined by the search speed of the separation matrix W, which should satisfy the condition that $\left\| W^T W \right| - 1 \right| \le \varepsilon$. Moreover, ε is a positive real variable and arbitrarily small.

For Fast ICA algorithm, the Newton iteration is taken into search for the optimized solution, with a superlinear convergence speed. On the other side, it takes random vectors of unity length for the initial separation matrix $\hat{W}$, which averagely needs more iteration to search separation matrix compared with Max-SINR ICA.

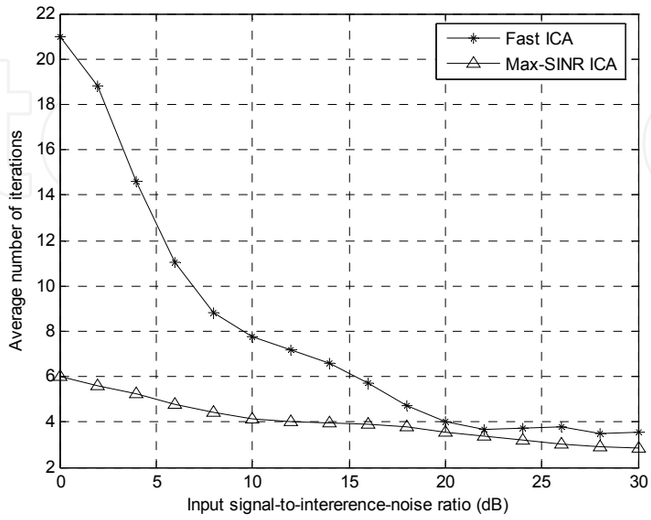


Fig. 17. Iterations of ICA algorithms

But for Max-SINR ICA algorithm, the analytical method is taken in searching for the initial separation matrix, which directly acquires a closed form solution by generalized eigenvalue decomposition. Then the Newton iteration is taken, which is based on the optimized initial separation matrix. Because there isn't an iterative process that search for the optimized initial separation matrix, its iterative steps are less than Fast ICA algorithm. Moreover, we can know from Theorem 1 that the initial $\hat{W}$ is an eigenvector matrix when SINR takes the maximum value in the objective function.

4.3.2 Fix the length of processing frame

In order to compare the performance of the introduced algorithm under different thermal noise, we fix the length of processing frame N , and let $N = 50$ symbols. In such situation, we only need to consider the effects of thermal noise in the mixed signals.
Furthermore, we give a definition about the output SNR (SNR_{out}) and the length of processing frame N , which is as the following equation.

$$SNR_{out} = 10\log\left\{\frac{1}{N}\sum_{k=1}^{N}\frac{u^2(k)}{[u(k)-\hat{u}(k)]^2}\right\} \tag{33}$$

In Eq. (33), $u(k)$ is the kth sample of useful signal $u(t)$, while $\hat{u}(k)$ is the estimated value of $u(k)$. On this basis, simulation is taken. The relationship of SNR_{out} and $SINR_{in}$ is illustrated in Fig. 17, where SNR_{out} is as a function of $SINR_{in}$ with different strength of thermal noise. Moreover, we select SNR_{in} to reflect the fluctuation of such strength. From Fig.17, it can be seen that SNR_{out} with both Max-SINR ICA algorithm and Fast ICA algorithm is robust with the increase of $SINR_{in}$.

As shown in Fig.18, we make $SINR_{in}$ vary from -10dB to 30dB, and SNR_{out} grows slowly with the increase of $SINR_{in}$. One reason is that the output SNR by ICA algorithm is affected by the mutual information among the source signals and the probability distribution of each signal. For such characteristics are determined, the limited change of $SINR_{in}$ plays a little effect in SNR_{out} .When SNR_{in} is equal to 40dB, SNR_{out} is around from 18dB to 22dB. But when SNR_{in} is equal to 10dB, SNR_{out} is around from 9dB to 14dB. Based on this analysis, it can be found that by means of ICA algorithm, the higher SNR_{in} is, the higher SNR_{out} is.

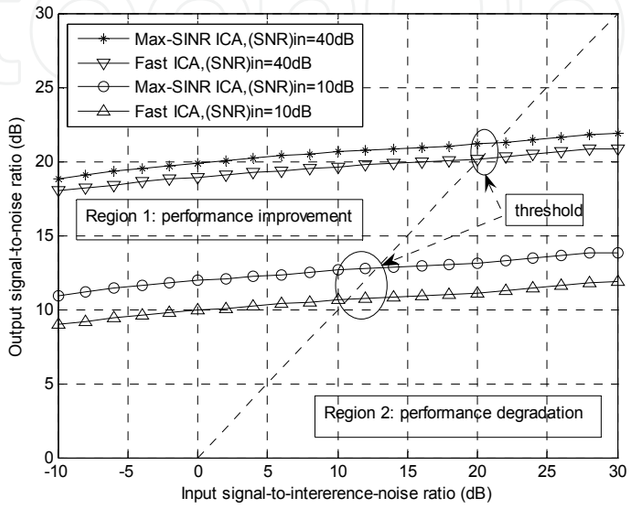


Fig. 18. SNR_{out} and $SINR_{in}$ (fix the length of processing frame)

On the other side, with the same condition, such as SNR_{in} is equal, the Max-SINR ICA algorithm shows a better performance than the Fast ICA algorithm. Especially, SNR_{out} improved by the Max-SINR ICA algorithm is a little more than SNR_{out} improved by the Fast ICA algorithm.

However, with the increase of $SINR_{in}$, the increase of SNR_{out} is still limited, whose growth rate is slower than $SINR_{in}$. As a result, when $SINR_{in}$ increases into some value, it reaches to balance: $SNR_{out} = SINR_{in}$. Moreover, this state is shown as the slash through the origin in Fig.18, which divides the graph into two regions: Region 1 and Region 2.

In Region 1, $SNR_{out} > SINR_{in}$, which means that the interference mitigation by ICA algorithm is effective. But in Region 2, $SNR_{out} < SINR_{in}$, which means that the interference mitigation by ICA algorithm is not only ineffective, but also degrades the performance worse as the growth of $SINR_{in}$.

Compared with the Fast ICA algorithm, the Max-SINR ICA algorithm raises the threshold $SINR_{in}$ of Region 1 and Region 2. It can be seen in Fig.18 that the threshold $SINR_{in}$ for the Max-SINR algorithm is a little larger, which means if $SINR_{in}$ is in this area, the performance is improved by the Max-SINR ICA algorithm, but degraded by the Fast ICA algorithm.

Fig. 19 shows the processing gain for such two ICA algorithms, when the length of processing frame is fixed. It can be found that the processing gain decreases with the increase of $SINR_{in}$. Besides, as $SINR_{in}$ continuously increases, we can set the area with the positive processing gain as Region 1, while the area with the negative processing gain as Region 2. Among Region 1 and Region 2 is the threshold line.

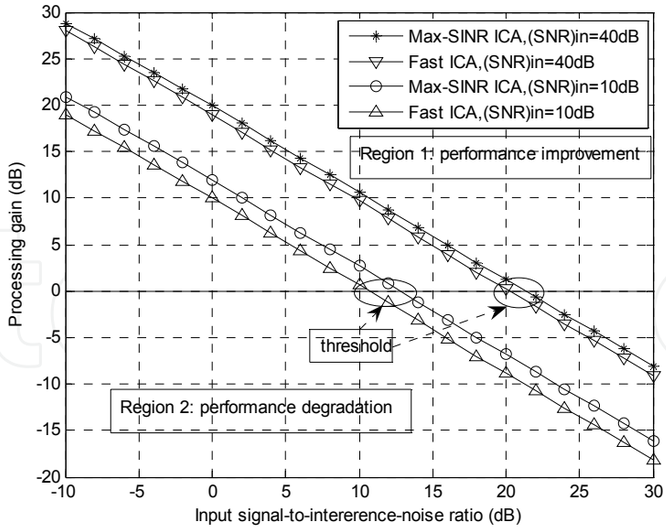


Fig. 19. Processing gain (fix the length of processing frame)

Specially, when $SINR_{in}$ is lower than the threshold, the processing gain is positive, which enables to improve the performance. What's important, the lower the $SINR_{in}$ is, the higher the processing gain is, which is useful to the users in cell-edge. But when $SINR_{in}$ is higher than the threshold, the processing gain is negative, which degrades the performance.

Compared with the performance brought by such two algorithms, the processing gain brought by the Max-SINR ICA algorithm is larger with the same SNR_{in}. Moreover, the introduced algorithm also raises the threshold $SINR_{in}$. When $SINR_{in}$ is among this area, the processing gain can be improved by the Max-SINR ICA algorithm, but degraded by the Fast ICA algorithm.

4.3.3 Fix the strength of thermal noise

In order to measure the effects brought by the length of processing frame, we fix the strength of thermal noise in the mixed signals, which is in a form of fixed signal to noise ratio, $SNR_{in} = 40dB$. Moreover, the simulation result is shown in Fig.20, and SNR_{out} is also set as a function of $SINR_{in}$ with different lengths of the processing frame.

In static simulation, we respectively take the length of the processing frame as 50 and 100, and the performance brought by such two ICA algorithms is compared. Further, it can be seen that the performance can be divided into two regions:

In Region 1, the performance is improved, where $SNR_{out} > SINR_{in}$. With the increase of $SINR_{in}$, it shows that for the same ICA algorithm, the longer the length of the processing frame is, the higher the SNR_{out} is. The reason is that the independence among source signals is easier to be established with longer processing frames. But in Region 2, the performance is degraded, where $SNR_{out} < SINR_{in}$, and it is degraded worse as $SINR_{in}$ increases gradually. Moreover, when the length of the processing frame is longer, the threshold $SINR_{in}$ between Region 1 and Region 2 also becomes a little higher.

The reason why Region 1 and Region 2 exist in Fig. 18 and Fig. 20 is that: The output SNR by ICA algorithm is mainly affected by the mutual information among the source signals and the probability distribution of each signal. Once such characteristics are determined in the

mixed signals, the limited change of $SINR_{in}$ plays a little effect in SNR_{out}. At this time, as the growth of $SINR_{in}$, SNR_{out} increases slowly, such curve may gradually reach to the threshold. Before this threshold, it's Region 1. Else, it's Region 2.

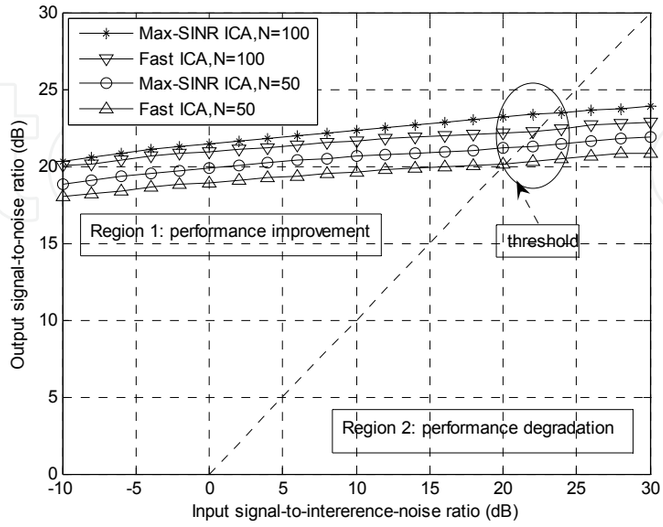


Fig. 20. SNR_{out} and $SINR_{in}$ (fix the strength of thermal noise)

Compared with the Fast ICA algorithm, both SNR_{out} and the threshold $SINR_{in}$ are raised by the Max-SINR ICA algorithm, with the same processing frame. From Fig. 20, it can be seen that in the threshold area, the performance is improved by the Max-SINR ICA algorithm, but degraded by the Fast ICA algorithm.

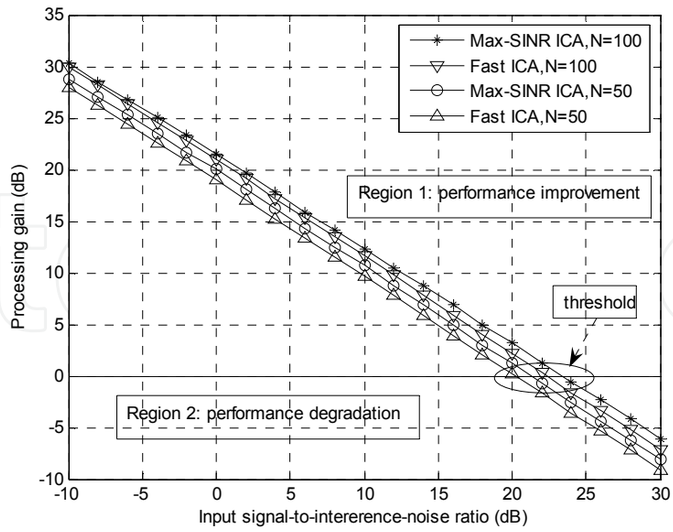


Fig. 21. Processing gain (fix the strength of thermal noise)

Fig.21 shows the processing gain for such two ICA algorithms, when the strength of thermal noise is fixed. It can be found that the processing gain decreases with the increase of $SINR_{in}$. In Region 1, the processing gain is positive, and enables to improve the performance. While

in Region 2, the processing gain is negative, and degrades the performance. Similar to Fig.19, it also can be found from Fig.21 that the longer the length of the processing frame is, the higher the processing gain is.

Compared with the Fast ICA algorithm, both the processing gain and the threshold are raised by the Max-SINR ICA algorithm with the same processing frame. The conventional Fast ICA has forced the interference to zero, not considering the effect of the additive thermal noise. Meanwhile, the introduced algorithm minimizes both the interference and noise in order to maximize SINR. Thus the effect of the noise enhancement can be suppressed by the introduced algorithm, which gives the performance improvement.

Based on the above analysis, it's proper to use ICA algorithm under lower $SINR_{in}$, higher SNR_{in} and with longer lengths of the processing frame, which enables to mitigate the inter-cell interference, and improve the performance. Specially, it had better employ such inter-cell interference algorithm in practical application when the range of $SINR_{in}$ is below 10dB, but SNR_{in} is above 10dB.

On the other side, it is worth noting that the effect of user mobility isn't considered because of static simulation. Actually, when the length of processing frame is too large, such mobility can't be tracked for the Doppler frequency effect and time varying channel. In practice, the length of processing frame should be limited by the maximum speed of UE, which need to be researched by dynamic simulation in the future.

4.4 Summary

In order to cancel inter-cell interference, one inter-cell interference mitigation method is introduced, which is based on ICA algorithm. Compared to finding the maximum kurtosis in classical ICA algorithms, such as Fast ICA, Max-SINR ICA algorithm is introduced, which sets SINR as the objective function in this algorithm. As an important measured factor in interference mitigation, it need try to make such function get the maximum value. By optimize the initial separation matrix in iterations, the convergence speed of this introduced algorithm is faster than Fast ICA algorithm. Furthermore, two situations are divided in simulation, which respectively fix the length of processing frame and fix the strength of thermal noise.

By means of ICA algorithm, the output SNR increases as the growth of the input SINR, but the processing gain gradually decreases as the growth of the input SINR. Moreover, the lower the SINR is, the higher the output SNR and the processing gain are.

On the other side, as the growth of the input SINR, there are two regions for the performance. When the input SINR is lower than the threshold, the performance is improved. But when the input SINR is higher than the threshold, the performance is degraded.

Besides, the effects brought by the thermal noise and the length of the processing frame are considered. When the input SNR is higher in the mixed signals, the output SNR is higher. When the length of the processing frame is longer, the output SNR is also higher. What's more, compared with the Fast ICA algorithm, the Max-SINR algorithm raises the output SNR and the processing gain in the same conditions.

According to the above comparison, it can be found that this inter-cell interference cancellation method is performed well with lower SINR. So it's good to improve the quality of service for users in cell-edge where is always in the state of lower SINR. Another advantage is that this algorithm can be performed in a semi-blind state, with no precise knowledge of source signal and channel information. Moreover, it may not bring with extra

interference, which is much better than many existing inter-cell interference cancellation algorithms.

5. Conclusion

In this chapter, the inter-cell interference mitigation for mobile communication system is analyzed and three kinds of solutions with inter-cell interference coordination, inter-cell interference prediction and inter-cell interference cancellation are introduced with system models, theoretical analyses and simulation results.

For interference coordination, Soft Fractional Frequency Reuse and Coordination Frequency Reuse schemes are introduced. Their frequency reuse factors are derived. Simulation results are provided to show the throughputs in cell-edge are efficiently improved compared with soft frequency reuse scheme.

The inter-cell interference prediction is an active interference mitigation method. The theoretical basis, which is the optimal estimation theory, is provided with including of two parts: time series and the optimal filter estimation. Besides, the steps of Box-Jenkins method are introduced in addition. The reliability is also analyzed by means of prediction accuracy, which is based on the relationship of the coherent time and the time delay.

For inter-cell interference cancellation, two major technologies are described in this chapter, which are space interference suppression and interference reconstruction/subtraction respectively. Based on the independent component analysis (ICA) technology in blind source separation, a semi-blind interference cancellation algorithm is introduced, named as Max-SINR ICA, which aims to improve the output SNR and optimize the initial iterative separation matrix. Simulation results show that the iterative convergence speed for Max-SINR ICA algorithm is faster than the traditional Fast-ICA algorithm. By the Max-SINR ICA algorithm, the inter-cell interference can be efficiently cancelled in a semi-blind state, especially with lower input SINR, higher input SNR and longer processing frame.

6. References

3GPP. (2005). R1-050507, Soft frequency reuse scheme for UTRAN LTE, Huawei. *3GPP TSG RAN WG1 Meeting* #41, Athens, Greece.

3GPP. (2005). R1-051396. Comparison of bit repetition and symbol repetition for inter-cell interference mitigation.

3GPP. (2006). R1-060416. Combining inter-cell-interference co-ordination/avoidance with cancellation in downlink and TP.

3GPP. (2006). R1-060518. TP for combining beam-forming with other inter-cell interference mitigation approaches.

3GPP. (2006). TR 25.814 v7.1.0, Physical layer aspects for evolved UTRA (Release 7).

3GPP. (2006). TR 25.913, Requirements for Evolved UTRA (E-UTRA) and Evolved UTRAN (E-UTRAN).

3GPP. (2007). TR 25.912. Feasibility Study for Evolved UTRA and UTRAN.

3GPP. (2008). R1-082024, A discussion on some technology components for LTE-Advanced, Ericsson. 3GPP TSGRAN WG1 #53, Kansas City, MO, USA.

3GPP. (2008). R1-083569, Further discussion on Inter-Cell Interference Mitigation through Limited Coordination, Samsung. 3GPP TSGRAN WG1 #54bits, Prague, Czech Republic.

3GPP. (2009). R1-091688, Potential gain of DL CoMP with joint transmission, NEC Group. 3GPP TSGRAN WG1 #57, San Francisco, USA.

3GPP. (2009).TR 36.814 v1.0.1, Further Advancements for E-UTRA Physical Layer Aspects (Release 9).

A. Hyvarienen, J. Karhunen, E. Oja. (2001). Independent Component Analysis, John Wiley and Sons.

Haipeng Le, Lei Zhang, Xin Zhang, and Dacheng Yang. (2007).A Novel Multi-Cell OFDMA System Structure using Fractional Frequency Reuse, In *Proc. of IEEE PIMRC* 2007, pp.1-5.

Hanbyul Seo and Byeong Gi Lee. (2004). A proportional-fair power allocation scheme for fair and efficient multiuser OFDM systems, In *Proc. of IEEE Globecom* '04 ,vol.6, pp.3737-3741.

H.L. Bertoni. (2000). Radio propagation for modern wireless systems. Prentice Hall, Inc.

Huiling Jia, Zhaoyang Zhang, Guanding Yu, Peng Cheng, and Shiju Li. (2007).On the Performance of IEEE 802.16 OFDMA System under Different Frequency Reuse and Subcarrier Permutation Patterns, In *Proc. of IEEE International conference on communications*, ICC 07', pp.5720-5725.

Hui Zhang, Xiaodong Xu, Xiaofeng Tao, Ping Zhang. (2009). An Inter-Cell Interference Mitigation Method for OFDM-Based Cellular Systems Using Independent Component Analysis. *IEICE Transactions on Communications*, Vol.E92-B, No.10.

Hui Zhang, Xiaodong Xu, Jingya Li, Xiaofeng Tao. (2009). Multicell Power Allocation Method based on Game Theory for Inter-Cell Interference Coordination. *Science in China, Series F: Information Sciences*, Vol.52, No.12, pp: 2378-2384.

Hui Zhang, Jingya Li, Xiaodong Xu, Shuang Wang, Ping Zhang. (2009). Multi-cell Subcarrier Allocation based on Interference Forecast by Kalman Filter. *Journal of Beijing University of Posts and Telecommunications*, Vol.32, No.3, pp.86-90.

Hui Zhang, Xiaodong Xu, Jingya Li, and Xiaofeng Tao.(2010) Subcarrier Resource Optimization for Cooperated Multipoint Transmission. *International Journal of Distributed Sensor Networks*, vol. 2010.

Hui Zhang, Jingya Li, Xiaodong Xu, Tommy Svensson. (2009). Channel Allocation based on Kalman Filter Prediction in Downlink OFDMA Systems. *IEEE VTC 2009*-Fall.

Hyvarinen, A. (1999). Fast and robust fixed-point algorithms for independent component analysis. *IEEE Trans. on Neural Networks*, vol.10, no. 3, pp. 626 - 634.

I. Kostanic, W. Mikhael. (2002).Rejection of the co-channel interference using non-coherent independent component analysis based receiver, *Proc. IEEE Midwest Symposium on Circuits and Systems*, vol. 2, Aug.2002.

I.Kostanic, W.Mikhael. (2004).Blind source separation technique for reduction of co-channel interference. *IEE Electronics Letters*, Vol. 38, No. 20, pp.1210 – 1211.

J.G.Andrews. (2005). Interference cancellation for cellular systems: a contemporary overview. *IEEE Wireless Commun*. Magazine, vol.12, no. 2, pp. 19 - 29.

J. Tomcik. (2006). Qualcomm, MBFDD and MB TDD wideband mode, *IEEE* 802.20-05/68r1.

K.N. Lau, K. Yu, K. Ricky.(2006). Channel adaptive technologies and cross layer designs for wireless systems with multiple antennas theory and applications. Canada: John Wiley & Sons, Inc., Publication, pp. 1-503.

K.I. Lee, Y.H. Ko. (2006). An inter-cell interference cancellation method for OFDM cellular systems using a subcarrier-based virtual MIMO. *Proc. IEEE VTC*, pp. 1-5.

Ki Tae Kim, Seong Keun Oh. (2007).A Universal Frequency Reuse System in a Mobile Cellular Environment, In *Proc. of IEEE VTC* 2007-Spring, pp.2855-2859.

Ki Tae Kim, Seong Keun Oh. (2008).An Incremental Frequency Reuse Scheme for an OFDMA Cellular System and Its Performance, In *Proc. of IEEE VTC* 2008-Spring, pp.1504-1508.

K.W. Park, K.I. Lee, Y.S. Cho. (2006). An inter-cell interference cancellation method for OFDM-Based cellular systems using a virtual smart antenna. *IEICE Trans. on Commun.*, vol. E89-B, no.1, pp. 217-219.

L. Prarra, P. Sajda.(2003). Blind source separation via generalized eigenvalue decomposition. *Journal of Machine Learning Research*, no.4, pp. 1261-1269.

M. Barkat. (2005). Signal Detection and Estimation. Artech House Publishers.

Q.H. Spencer, C.B. Peel. (2004). An introduction to the multi-user MIMO downlink. *IEEE Commun. Magazine*, vol.42, pp. 60-67.

S.E. Elayoubi, O. B. Haddada, and B. Fourestie. (2008). Performance Evaluation of Frequency Planning Schemes in OFDMA-based Networks, *IEEE Trans. Wireless Commun.*, vol. 7, no.5, pp. 1623–1633.

S.R. Curnew, J. How. (2007). Blind signal separation in MIMO OFDM systems using ICA and fractional sampling. *Proc. International Symposium on Signals, Systems and Electronics*, pp. 67-70.

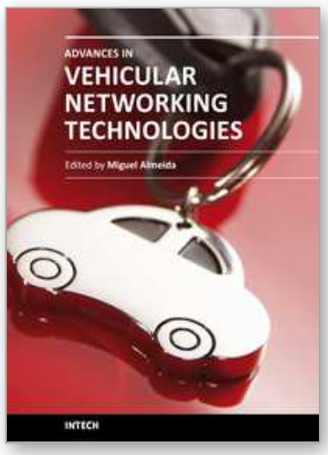
T. Ristaniemi, J. Joutsensalo. (1999). Nonlinear algorithm for blind interference cancellation, *Proc. IEEE Signal Processing Workshop on Higher-Order Statistics*, pp.43-47.

T. Yang. (2004). Diversity wireless receivers with efficient co-channel interference suppression. *Proc. IEEE Advances in Wired and Wireless Communication*, pp.145-147.

Xu Fangmin, Tao Xiaofeng, Zhang Ping. (2009). A Frequency Reuse Scheme for OFDMA Systems, *Journal of Electronics&Information Technology*,vol. 3, no.4, pp.903-906.

Xu Xiaodong, Zhang Hui, Li Jingya, Tao Xiaofeng, Zhang Ping. (2009). An Improved Exponential Distributed Power Control Algorithm for MIMO Cellular Systems. *IEEE WiCOM* 2009.

IntechOpen



Advances in Vehicular Networking Technologies

Edited by Dr Miguel Almeida

ISBN 978-953-307-241-8
Hard cover, 432 pages
Publisher InTech
Published online 11, April, 2011
Published in print edition April, 2011

This book provides an insight on both the challenges and the technological solutions of several approaches, which allow connecting vehicles between each other and with the network. It underlines the trends on networking capabilities and their issues, further focusing on the MAC and Physical layer challenges. Ranging from the advances on radio access technologies to intelligent mechanisms deployed to enhance cooperative communications, cognitive radio and multiple antenna systems have been given particular highlight.

How to reference

In order to correctly reference this scholarly work, feel free to copy and paste the following:

Xiaodong Xu, Hui Zhang and Qiang Wang (2011). Inter-cell Interference Mitigation for Mobile Communication System, Advances in Vehicular Networking Technologies, Dr Miguel Almeida (Ed.), ISBN: 978-953-307-241-8, InTech, Available from: http://www.intechopen.com/books/advances-in-vehicular-networking-technologies/inter-cell-interference-mitigation-for-mobile-communication-system

INTECH
open science | open minds

InTech Europe
University Campus STeP Ri
Slavka Krautzeka 83/A
51000 Rijeka, Croatia
Phone: +385 (51) 770 447
Fax: +385 (51) 686 166
www.intechopen.com

InTech China
Unit 405, Office Block, Hotel Equatorial Shanghai
No.65, Yan An Road (West), Shanghai, 200040, China
中国上海市延安西路65号上海国际贵都大饭店办公楼405单元
Phone: +86-21-62489820
Fax: +86-21-62489821

© 2011 The Author(s). Licensee IntechOpen. This chapter is distributed under the terms of the Creative Commons Attribution-NonCommercial-ShareAlike-3.0 License, which permits use, distribution and reproduction for non-commercial purposes, provided the original is properly cited and derivative works building on this content are distributed under the same license.

IntechOpen

IntechOpen